BMC Microbiology

RESEARCH

Open Access

High-throughput single-cell analysis reveals fully human Omp38-specific monoclonal antibodies against *Acinetobacter baumannii*

Yiwei Zhang[1†], Wenkang Yu[2†], Peng Yu[3], Shufeng Wang[1], Hui Dong[1], Yong Qi[4], Xiaohua Chen[4], Li Zhang[5], Yuxiang Liu[6], Xing Mou[6], Tingting Zhao[3], Jingbo Zhang[7], Xiangmei Chen[8], Haibo Li[2*], Shun Zhou[6*], Yuzhang Wu[1,3*] and Yi Tian[1*]

Abstract

Background *Acinetobacter baumannii (A. baumannii)* is a significant global health threat, particularly in hospital environments, where it is often linked to severe infections. As the need for innovative therapeutic approaches grows, fully human monoclonal antibodies (mAbs) have gained attention because of their high specificity, reduced immunogenicity, and enhanced affinity for target antigens, which may improve clinical efficacy.

Methods Using the Beacon platform, we isolated single B cells from immunized humanized genomic orthologs for antibody development (HUGO-Ab) mice to develop outer membrane protein (OMP)-specific mAbs. The variable regions of the selected mAbs were cloned into mammalian expression vectors containing constant human IgG1 regions to generate fully human mAbs. After identifying mAbs binding to Omp38 via ELISA, their binding ability to LAC-4 and the clinical isolates was further evaluated. Subsequently, the effects of these mAbs on *A. baumannii* adhesion and biofilm formation were tested, and their protective efficacy was assessed using a lethal infection model. Finally, bioinformatics methods were used to predict the binding conformation of mAb F2 to Omp38.

Results Omp38-specific fully human mAb F2 potently and broadly bound to *A. baumannii* strains and inhibited bacterial adherence and biofilm formation. Binding modeling and conformational analysis revealed that F2 targets the extracellular region of Omp38 and forms stable hydrogen bonds with different strains, suggesting its potential for broad-spectrum binding to diverse *A. baumannii* strains.

†Yiwei Zhang and Wenkang Yu contributed equally to this work.

*Correspondence:
Haibo Li
lihaibo@tmmu.edu.cn
Shun Zhou
shawnzhou@cyagen.com
Yuzhang Wu
wuyuzhang@tmmu.edu.cn; wuyuzhang@iiicq.vip
Yi Tian
tianyi@tmmu.edu.cn

Full list of author information is available at the end of the article

Conclusions This study demonstrates the utility of high-throughput single-cell analysis and antibody engineering in developing fully human mAbs against *A. baumannii*, highlighting the potential of these novel fully human mAbs to advance therapeutic strategies and improve clinical outcomes for *A. baumannii* infections.

Keywords *Acinetobacter baumannii*, Outer membrane protein, Fully human monoclonal antibody, Beacon

Background

Acinetobacter baumannii (A. baumannii) has emerged as a significant threat in healthcare settings, known for its role in severe opportunistic infections, particularly among immunocompromised patients and in intensive care units (ICUs) [1, 2]. This pathogen is notorious for its profound ability to acquire antimicrobial resistance, leading to infections that are difficult to treat and resulting in substantial morbidity and mortality [1, 2].

Standard treatment regimens often include a combination of broad-spectrum antibiotics; however, this approach can lead to suboptimal outcomes, prolonged hospital stays, and increased mortality rates, especially in immunocompromised patients [3, 4]. Additionally, the emergence of multidrug-resistant strains poses a serious threat to effective treatment options [3, 4]. Monoclonal antibody (mAb) therapy has several advantages over traditional antibiotics, including high specificity to their targets, increased therapeutic predictability, and a lower likelihood of adverse side effects due to reduced off-target activity [5]. Moreover, mAbs can be engineered to improve their pharmacokinetics, enabling prolonged biological activity and retention in circulation [6].

The earliest mAbs were mouse-derived antibodies invented by G Köhler and C Milstein in 1975 [7, 8]. However, because the constant region of mouse-derived mAbs is recognized by the human immune system, the vast majority (up to 80%) of patients who receive mouse-derived mAb therapy develop anti-murine antibody responses (human anti-mouse antibody, HAMA) [9, 10]. In contrast, humanized mAbs provide significant advantages by minimizing immunogenic risks while retaining the ability to bind to target antigens with high specificity [11, 12]. With the development of fully human mAbs, the efficacy and safety of the treatment of various infections have improved [13, 14]. In recent years, in vitro technologies such as phage display, ribosome display, and mRNA display have emerged that generate fully human antibodies from antibody gene libraries, which can even surpass the natural human antibody repertoire [15]. However, mAbs produced using these in vitro methods tend to have relatively low affinity, as they have not undergone processes such as affinity maturation [16]. Recent studies have shown that advancements have been made in techniques utilizing transgenic animals with a human antibody gene repertoire to obtain fully human antibodies [15, 17]. This approach allows for the integration of modern recombinant DNA technologies with well-established immunization techniques to produce affinity-matured human antibodies [15, 18].

A. baumannii possesses a diverse array of protein targets with potential therapeutic implications, among which Omp38 stands out as a particularly significant OMP [1, 19, 20]. It plays a crucial role in mediating bacterial adhesion, invasion, and biofilm formation [1, 19, 20]. Furthermore, Omp38 modulates inflammatory responses and influences various aspects of host immune defense mechanisms [1, 21]. Our previous study developed Omp38-specific murine mAbs in a high-throughput manner and found that the mAbs played an important role against *A. baumannii* infection [22]. However, no studies have focused on fully humanized mAbs against Omp38.

In this study, we immunized humanized genomic orthologs for antibody development (HUGO-Ab) mice with outer membrane proteins (OMP) and then utilized the Beacon platform for high-throughput single B cell isolation as previously described [22], which facilitates the identification and selection of high-affinity antibodies directly from the immune repertoire of the mice. Subsequently, we confirmed the binding activity and impact of these mAbs on bacterial invasiveness. Through these innovative approaches, Omp38-sepcific fully human mAbs may contribute to improved treatment outcomes for *A. baumannii* infections in clinical settings.

Methods

Ethics statement

Ethical approval was obtained from the Animal Ethics and Experimental Committee of the Army Medical University in Chongqing, China (Approval No. 20250017). All surgical instruments and the operating environment were maintained under sterile conditions to minimize the risk of infections. Surgical procedures were conducted by skilled personnel to ensure operational precision, minimize bleeding, and reduce tissue trauma in mice.

Cells, animals and bacterial strains

ExpiCHO cells were cultured in MetaCell CHO-310 medium (Cellplus Bio, Catalog No. L1013). Six-to eight-week-old specific pathogen-free (SPF) female C57BL/6 mice were obtained from the Experimental Animal Center of Army Medical University. The HUGO-Ab mouse was developed based on Cyagen's proprietary TurboKnockout ES targeting technology. It features the replacement of the mouse heavy chain, kappa light

chain, and lambda light chain V(D)J genes with human sequences and is designed for the discovery of fully human antibodies.

All mice were housed under SPF conditions in the animal care facility of the Army Medical University. *A. baumannii* strains ATCC 17,978 and LAC-4 were generously supplied by Prof. Haibo Li from the Department of Microbiology and Biochemical Pharmacy at Army Medical University. Clinical *A. baumannii* strains were collected from the General Hospital of the Central Theater Command. The sequence types (STs) of *A. baumannii* strains were identified as previously described [22]. Subsequently, we performed BLAST alignment of genomic sequences obtained from next-generation sequencing of clinical *A. baumannii* strains against the Comprehensive Antimicrobial Resistance Database (CARD) to obtain the corresponding antimicrobial resistance functional annotations. We ranked all antibiotic resistance genes by percent identity (in descending order) against the CARD database references and focused on the top five highest-ranking genes (each exhibiting > 97% identity) (Table 1). Notably, all identified genes showed perfect matches with *Acinetobacter*. Moreover, all alignments were supported by E-values < 1.0E-5, further reinforcing the reliability of our annotation (Table 1).

Mouse immunization

A total of 50 μg of OMPs was combined with 50 μL of QuickAntibody Mouse3W (Biodragon, Catalog No. KX0210042) were intramuscularly injected into the calf muscles of 6–8-week-old HUGO-Ab mice on days 0, 14, and 21 [22]. On day 21, a minor blood sample was collected from the tail vein to determine the serum OMP antibody titer using an enzyme-linked immunosorbent assay (ELISA) [22]. The mouse with the highest anti-OMP polyclonal antibody titer was selected for further experimental procedures. Furthermore, a final booster injection was delivered intraperitoneally three days before conducting assessments using the Beacon system.

Isolation of single OMP-specific antibody-secreting cells (ASCs) via the Berkeley lights beacon system

Before performing the on-chip assay, biotinylated outer membrane proteins (OMPs) were immobilized onto streptavidin-functionalized assay beads (Berkeley Lights, 520 – 00053) through overnight incubation at 4 °C [22]. The conjugated beads were subsequently mixed with a fluorescently labeled anti-mouse secondary antibody (Alexa Fluor 568, Thermo Fisher, A-11004) at a dilution of 1:100 [22].

The ASCs were then loaded onto OptoSelect 11k chips and cultured at 25 °C in a specialized plasmablast survival medium (Berkeley Lights, 75002051) formulated to enhance antibody secretion while preserving cell viability [22–24]. Single-cell encapsulation was achieved using optoelectropositioning (OEP) technology, allowing for the optical transfer of ASCs into nanoliter-sized chambers referred to as NanoPens. This light-based manipulation technique enabled the distribution of thousands of ASCs across multiple chips into NanoPens [22]. A fluorescence-based on-chip assay was conducted to identify antibodies binding to the OMPs, with fluorescence intensity measurements recorded at 5-minute intervals for a total duration of 20 min under controlled conditions at 36 ℃ [22]. OMP-specific antibody-producing cells were identified within NanoPens [22]. After isolating and transferring antigen-specific B cells from the NanoPens using opto-electro-positioning (OEP), the microfluidic chips were rinsed with culture medium for 2 min per cell. Subsequently, the cells were exported into wells of 96-well RT-PCR plates preloaded with lysis buffer (Qiagen, 1070498) and maintained at 25 ℃ [22].

Single B-cell sequencing and plasmid construction

After being exported from the Beacon system, the VH and VL sequences of antibodies secreted by OMP-binding B cells were amplified using reagents provided in the Opto Plasma B Discovery cDNA Synthesis Kit (Berkeley Lights, 750–02030) [22]. RNA was extracted and purified from single B cells using Agencourt RNAClean XP beads (Beckman Coulter, A63987) [22]. Subsequently, first-strand cDNA synthesis and total cDNA amplification were performed according to the manufacturer's protocol (Berkeley Lights, 750–02030). The amplified total cDNA was purified using Agencourt AMPure XP beads (Beckman Coulter, A63881) and subsequently prepared for sequencing using the Opto Plasma B Discovery Sanger Prep Kit (Berkeley Lights, 750–02041) [22]. Sanger sequencing was used to determine the nucleotide sequences of the amplified products [22]. VH, VL, and complementarity-determining region 3 (CDR3) sequences, as well as somatic hypermutation frequencies, were analyzed using Geneious Prime (version 2021.0.3) and the IMGT database (https://www.imgt.org/). The paired VH and VL sequences for the selected mAbs were codon-optimized, synthesized by Shenggong Biotech, and subsequently cloned into separate mammalian expression vectors carrying constant human IgG1 regions to develop fully human mAbs.

mAb expression and purification

ExpiCHO cells were cultured to achieve a density of approximately 8×10^6 to 1×10^7 cells/mL, while maintaining a viability rate exceeding 98% [22]. The vectors were transfected into 2×10^8 ExpiCHO cells using equal volumes of electroporation buffer parts A and B (Celetrix, 1228), followed by incubation at 37 ℃ in a 7% CO_2 environment. At 18–22 h post-transfection (day 1), the

Table 1 Annotation of antimicrobial resistance genes in clinical A. baumannii strains

Strain Name	ARO_Name	Gene Family	Resistance Mechanism	percent identity	E-value
Strain 1	adeK	resistance-nodulation-cell division (RND) antibiotic efflux pump	antibiotic efflux	100	0
	ADC-156	ADC beta-lactamases pending classification for carbapenemase activity	antibiotic inactivation	100	1.72E-287
	adeL	resistance-nodulation-cell division (RND) antibiotic efflux pump	antibiotic efflux	100	1.9E-251
	Acinetobacter baumannii AbaQ	major facilitator superfamily (MFS) antibiotic efflux pump	antibiotic efflux	100	2.28E-234
	OXA-120	OXA beta-lactamase	antibiotic inactivation	100	5.33E-202
Strain 2	ADC-70	ADC beta-lactamases pending classification for carbapenemase activity	antibiotic inactivation	100	4.22E-288
	OXA-417	OXA beta-lactamase	antibiotic inactivation	100	1.21E-202
	Acinetobacter baumannii AbaQ	major facilitator superfamily (MFS) antibiotic efflux pump	antibiotic efflux	98.8	6.88e-313
	adeI	resistance-nodulation-cell division (RND) antibiotic efflux pump	antibiotic efflux	98.1	5.22E-278
	adeK	resistance-nodulation-cell division (RND) antibiotic efflux pump	antibiotic efflux	97.5	0
Strain 3	adeK	resistance-nodulation-cell division (RND) antibiotic efflux pump	antibiotic efflux	100	0
	adeC	resistance-nodulation-cell division (RND) antibiotic efflux pump	antibiotic efflux	100	0
	Acinetobacter baumannii AbaQ	major facilitator superfamily (MFS) antibiotic efflux pump	antibiotic efflux	100	1.02e-314
	Acinetobacter baumannii AbaF	major facilitator superfamily (MFS) antibiotic efflux pump	antibiotic efflux	100	1.55e-311
	adeI	resistance-nodulation-cell division (RND) antibiotic efflux pump	antibiotic efflux	100	3.59E-283
Strain 4	adeK	resistance-nodulation-cell division (RND) antibiotic efflux pump	antibiotic efflux	100	0
	adeC	resistance-nodulation-cell division (RND) antibiotic efflux pump	antibiotic efflux	100	0
	Acinetobacter baumannii AbaQ	major facilitator superfamily (MFS) antibiotic efflux pump	antibiotic efflux	100	1.02e-314
	Acinetobacter baumannii AbaF	major facilitator superfamily (MFS) antibiotic efflux pump	antibiotic efflux	100	1.55e-311
	adeI	resistance-nodulation-cell division (RND) antibiotic efflux pump	antibiotic efflux	100	3.59E-283
Strain 5	adeK	resistance-nodulation-cell division (RND) antibiotic efflux pump	antibiotic efflux	100	0
	adeC	resistance-nodulation-cell division (RND) antibiotic efflux pump	antibiotic efflux	100	0
	Acinetobacter baumannii AbaQ	major facilitator superfamily (MFS) antibiotic efflux pump	antibiotic efflux	100	1.02e-314
	Acinetobacter baumannii AbaF	major facilitator superfamily (MFS) antibiotic efflux pump	antibiotic efflux	100	1.55e-311
	adeI	resistance-nodulation-cell division (RND) antibiotic efflux pump	antibiotic efflux	100	3.59E-283
Strain 6	ADC-18	ADC beta-lactamase without carbapenemase activity	antibiotic inactivation	100	1.72E-287
	OXA-272	OXA beta-lactamase	antibiotic inactivation	100	1.72E-202
	Acinetobacter baumannii AbaQ	major facilitator superfamily (MFS) antibiotic efflux pump	antibiotic efflux	99.8	1.45e-314
	tet(39)	major facilitator superfamily (MFS) antibiotic efflux pump	antibiotic efflux	99.5	2.05E-276
	adeI	resistance-nodulation-cell division (RND) antibiotic efflux pump	antibiotic efflux	98.1	5.22E-278
Strain 7	adeK	resistance-nodulation-cell division (RND) antibiotic efflux pump	antibiotic efflux	100	0
	adeC	resistance-nodulation-cell division (RND) antibiotic efflux pump	antibiotic efflux	100	0
	Acinetobacter baumannii AbaQ	major facilitator superfamily (MFS) antibiotic efflux pump	antibiotic efflux	100	1.02e-314
	Acinetobacter baumannii AbaF	major facilitator superfamily (MFS) antibiotic efflux pump	antibiotic efflux	100	1.55e-311
	adeI	resistance-nodulation-cell division (RND) antibiotic efflux pump	antibiotic efflux	100	3.59E-283

Table 1 (continued)

Strain Name	ARO_Name	Gene Family	Resistance Mechanism	percent identity	E-value
Strain 8	adeK	resistance-nodulation-cell division (RND) antibiotic efflux pump	antibiotic efflux	100	0
	adeI	resistance-nodulation-cell division (RND) antibiotic efflux pump	antibiotic efflux	100	3.59E-283
	ADC-169	ADC beta-lactamases pending classification for carbapenemase activity	antibiotic inactivation	100	6.99E-287
	adeL	resistance-nodulation-cell division (RND) antibiotic efflux pump	antibiotic efflux	100	1.9E-251
	OXA-125	OXA beta-lactamase	antibiotic inactivation	100	1.53E-201
Strain 9	adeK	resistance-nodulation-cell division (RND) antibiotic efflux pump	antibiotic efflux	100	0
	adeC	resistance-nodulation-cell division (RND) antibiotic efflux pump	antibiotic efflux	100	0
	Acinetobacter baumannii AbaQ	major facilitator superfamily (MFS) antibiotic efflux pump	antibiotic efflux	100	1.02e-314
	Acinetobacter baumannii AbaF	major facilitator superfamily (MFS) antibiotic efflux pump	antibiotic efflux	100	1.55e-311
	adeI	resistance-nodulation-cell division (RND) antibiotic efflux pump	antibiotic efflux	100	3.59E-283

cell culture media was supplemented with 10% MetaCell CHO TransFeed (Cellplus Bio, L1008) and 0.7% MetaCell Tier Enhancer (Cellplus Bio, L1009) [22]. After a 5-day incubation period, samples with viable cell densities exceeding 50% and cell viability rates above 60% were harvested, and the supernatants were purified using Pierce centrifuge columns (Thermo Scientific, 89898) [22]. T The bound mAbs were washed with a buffer (5× sample volume) containing 100 mM Pro-Ac (pH 3.5). The pH of each sample was then adjusted to 5.0 using 0.5 M arginine [22]. The samples were concentrated using 50 kDa molecular weight cutoff (MWCO) membrane centrifugal filter units (Millipore, UFC905008) and centrifuged at 3500 × g for 3 min. Subsequently, the samples were filtered through a 0.22 μm membrane filter (Millipore, GSWP04700) [22]. The yield of purified mAbs was quantified using a BCA protein assay kit (Beyotime, P0012), and their purity was confirmed by SDS-PAGE and size-exclusion chromatography coupled with high-performance liquid chromatography (SEC-HPLC). Purified mAbs were stored at −80 °C for long-term preservation.

ELISA

A total of 0.4 μg of recombinant Omp38 or 1×10^7 colony-forming units (CFUs) of *A. baumannii* were added to each well of 96-well ELISA plates (LABSELECT, 31111) and incubated overnight at 4 °C [22]. The plates were washed three times with phosphate-buffered saline (PBS) containing 0.05% Tween 20 (Sigma-Aldrich, P3563), followed by blocking with 2% fetal bovine serum (FBS) (Gibco, A5669701) in PBS for 1 h [22]. After blocking, the plates were washed three times. Serial dilutions of either recombinant mAb or isotype control mAb (MedChemExpress, HY-P99001) were added to the wells, and the plates were incubated at 37 ℃ for 1 h [22]. Following three washes, horseradish peroxidase (HRP)-conjugated goat anti-human IgG (H + L) (AB Clonal, AS002) was added and incubated at 37 ℃ for an additional hour. The enzymatic reaction was initiated by adding 3,3',5,5'-tetramethylbenzidine (TMB) substrate (Beyotime, P0209), and color development was allowed to proceed in the dark. The reaction was terminated by adding 1 N hydrochloric acid, and the absorbance was measured at 450 nm wavelength. The half-maximal effective concentration (EC_{50}) was determined using a four-parameter nonlinear regression model.

A. baumannii adherence assay

A. baumannii adherence assay was performed following previously established protocols [19, 22, 25]. *A. baumannii* ATCC 17,978 was cultured overnight in 10 mL of Luria–Bertani (LB) medium at 37 ℃ with moderate shaking at 175 rpm. The bacterial suspensions were washed with PBS and adjusted to approximately 1.0×10^9 CFU/mL. After A549 cells adhered to the plate, the complete Ham's F-12 K (Kaighn's) medium was replaced with culture medium containing heat-inactivated FBS (incubated at 56 ℃ for 30 min) and preincubated at 37 ℃ for 30 min to eliminate complement interference. The cells were then infected with live *A. baumannii* ATCC 17,978 at a multiplicity of infection (MOI) of 1:100. Subsequently, either mAb or isotype control was added. The infected cells were incubated at 37 ℃ in a 5% CO_2 atmosphere for 90 min. To quantify the adherent bacteria, nonadherent bacteria were removed by washing the cells four times with PBS. The cells were then lysed by adding 100 μL of 1% Triton X-100 in PBS per well [19], and the number of adherent bacteria was determined using the serial dilution method.

Biofilm inhibition assay

The biofilm inhibition assay was conducted according to the methodology outlined in previous studies [19, 22]. *A.*

baumannii ATCC 17,978 was cultured overnight in 10 mL of Luria–Bertani (LB) medium at 37 ℃ with moderate shaking at 175 rpm. The bacterial suspensions were washed with PBS and adjusted to approximately 1.0×10^7 CFU/mL. In each well of a 96-well polystyrene plate, 180 µL of the bacterial suspension and 20 µL of mAb was combined. The edges of the plate were sealed with film, and the plate was incubated at 37 ℃ for 26 h to facilitate biofilm formation. After incubation, the biofilm was fixed by adding 120 µL of methanol to each well for 20 min. The bacterial suspension was carefully aspirated, and the plate was washed twice with deionized water, followed by air-drying for 4 h. Subsequently, 150 µL of 0.1% crystal violet stain was added to each well, and the samples were stained for 30 min. The crystal violet solution was removed, and the wells were rinsed thoroughly with physiological saline until the wash solution became colorless. The plate was then air-dried overnight. To solubilize the biofilm, 120 µL of 95% ethanol was added to each well, and the plate was incubated at room temperature for 30 min. Finally, the absorbance was measured at 600 nm using a microplate reader.

Mouse model

Prior to the formal experiments, we conducted a series of dose-ranging studies and confirmed that the optimal challenge dose of LAC-4 was 1.4×10^7 CFU (Figure S1). C57BL/6 mice were anesthetized by intraperitoneal administration of pentobarbital sodium at a dosage of 50 mg/kg. Following anesthesia, the mice were challenged with a lethal dose of 1.4×10^7 CFU of LAC-4 suspended in 20 µL of PBS, delivered via noninvasive intratracheal inoculation, as previously described [22, 26, 27]. Immediately after inoculation, the mice were intravenously treated with mAbs. LAC-4 was quantified and verified using a serial dilution method. To assess survival rates in mice with lethal *A. baumannii* infection, seven mice from each group were anesthetized through intraperitoneal administration of sodium pentobarbital at a dosage of 50 mg/kg to guarantee that the animals were unconscious and unaware during the procedure and then euthanized by cervical dislocation 72 h postinfection.

Analysis of the mAb binding conformation

This study employed two protein structure prediction platforms, AlphaFold3 and GeoBiologics, to generate a three-dimensional structural model of the antigen-antibody complex between the Omp38-specific mAb F2 and the Omp38 protein of a reference strain of *A. baumannii* (ATG88079.1) from the NCBI GenBank database. Building upon the antigen-antibody complex structures predicted by AlphaFold3 and GeoBiologics, the "Build Homology Models" module in Discovery Studio 2.5 was used to construct the antigen-antibody complex structures of Omp38 and mAb F2 from other strains. In the calculation of interaction energy, the loop regions of the antigen and the variable region of the antibody within the antigen-antibody complex structure were designated as the interaction regions, whereas the remaining regions were considered as "fixed." The "Standard Dynamic Cascade" function in Discovery Studio 2.5 was applied to perform energy minimization and molecular dynamics calculations using the CHARMm force field. Energy minimization was accomplished through the sequential use of the "Steepest Descent" and "Conjugate Gradient" methods until the root-mean-square (RMS) gradient reached 0.1. Subsequently, a 5000 picosecond (ps) equilibration process was conducted at 300 K, with the other parameters set to their default values. For the result output, the structures from the last 1000 ps of the dynamic calculation were extracted, with one conformation saved every 10 ps, yielding a total of 100 conformations. The "Calculate Interaction Energy Protocol" integrated in Discovery Studio 2.5 was employed to determine the interaction energy between the antigen and antibody, using "Implicit Distance-dependent Dielectrics" as the dielectric constant. The average interaction energy of the 100 output conformations was used to assess the strength of the interaction forces between the antibody and different antigens, and the conformation with the lowest energy among the output conformations was selected as the final complex.

Statistical analysis

Statistical analyses were performed using GraphPad Prism 8.0. Comparisons between the two groups were performed using Student's t-test. Survival rates across groups were evaluated using the log-rank (Mantel–Cox) test. Data are expressed as mean ± standard error of the mean (SEMs). Statistical significance was set at $P < 0.05$.

Results

High-throughput analysis of the single B-cell secretion of OMP-specific mAbs from HUGO-Ab mouse

OMP was obtained as described in our previous study [22]. Compared with the non-immunized group, the titers of OMP-specific polyclonal antibodies in the OMP-immunized group were higher after three rounds of OMP immunization (Fig. 1A and B).

Three days after the final boosting immunization with OMP protein, bone marrow and spleen cells were collected from the immunized mice. Plasma cells from immunized mice were enriched and loaded into the Berkeley Lights Beacon optofluidic system, where they were maintained in a supportive medium to ensure cell viability. High-throughput single-cell analysis confirmed that 9021 cells were successfully introduced into the individual NanoPens on the device chip (Figure S2A). Each

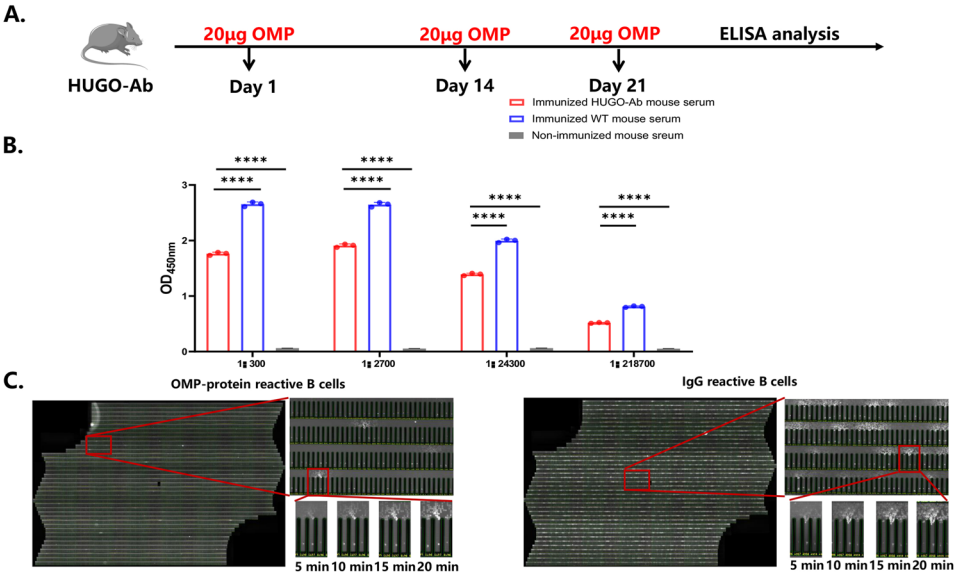

D.

mAb	VDJ Heavy	V region identity(%)	VH CDR1	VH CDR2	VH CDR3
F2	VH3-21/JH6/DH3-10	100	GYTFTRYVIH	WINAGNGNTK	AGMDV
A7	VH3-7/JH4/DH2-21	97.22	GFTFSTYWMS	NIKQDGSEKY	GLIAY
B2	VH4-39/JH5/DH3-10	98.28	GGSIRSSSNYWA	WIGSIYYSGSTY	GGVRGVLNWFDP
B3	VH4-4/JH6/DH3-10	97.22	GGSISSSDWWS	EIYHSGSTN	SGYYESGSFDYYHGLDV
B4	VH5-10-1/JH4/DH5-18	99.65	GYSFTSYWIS	RIDPSDFYTN	TRGYSDF
B6	VH3-7/JH4/DH3-16	97.92	GFTFSTYWMS	NIKQDGSEKY	GLIAY
B7	VH3-7/JH4/DH3-16	98.61	GFTFSTYWMS	NIKQDGSEKY	GLIAY
C4	VH6-1/JH3/DH3-10	99.33	GDSVSSNSAAWS	RTYYRSKWYND	LRITMVRRIIIYDTFDI
C7	VH3-20/JH6/DH3-10	97.22	GFTFDDYGMS	GINWNGGSKG	DRKRTHYYFKGLDV
D1	VH4-34/JH5/DH1-26	97.54	GGSFSGHYWS	EINHSESTN	GRVGATNWFDP
D4	VH3-48/JH6/DH2-2	96.88	GFTFSSYSMN	YISSSSSLIY	HMDV
D8	VH3-23/JH4/DH3-10	94.44	GFTFSSYAMR	VISGSGTSTY	ENGGFGELADF
E2	VH3-21/JH6/DH3-10	80.95	GFTFSSYSMN	SISSSSSYIY	NGYYYGSGSPYGMDV
E3	VH1-3/JH4/DH3-16	95.83	GYTFTNYAIH	WINAGKGNTE	EGDYVGGNYRPPFDY
E5	VH4-34/JH6/DH3-9	99.3	GGSFSGYYWS	EINHSGSTN	GPYYDILTGYYYGMDV
E7	VH1-3/JH4/DH3-16	96.53	GYTFTSYAIH	WINAGNGDTA	EGDYVWGNYRPPFDY
F3	VH4-61/JH5DH2-2	98.97	GGSVSSGRYYWS	YIYYSGSTN	EDCSSTNCYARWFDP
F4	VH6-1/JH6/DH5-12	95.96	GDSVASNSATWN	RTYYRSKWNND	GVATNRGYRYYYEMDV
F6	VH3-20/JH6/DH1-14	97.57	GFTFDDYGMS	GINWNGGSKG	DRKRTHYYFYGLDV
G4	VH1-3/JH4/DH3-16	95.83	GYIFTSYAIH	WINAGNGDTE	EGDYVWGGYRPPFDY
G7	VH6-1/JH6/DH5-12	94.61	GDIVSTNSATWN	RTYYRSKWKND	GVATNRGYQYFYEMDV
H2	VH1-3/JH4/DH3-16	89.58	GYTFTNYAIH	WINAGKGNTE	EGDYVGGNYRPPFDY
H3	VH3-7/JH4/DH3-16	96.53	GLNFSTYWMS	NIKQDGSEKY	GLIAY
H4	VH1-3/JH4/DH3-16	95.49	GYTFTNYAIH	WINAGKGNTE	EGDYVGGNYRPPFDY

mAb	VJ Light	V region identity(%)	VL CDR1	VL CDR2	VL CDR3
F2	VK1-6/JK1	100	RSSQSLVYSDGDTYLN	KVSNRDS	MQGTHWPLT
A7	VL7-46/JL3	65.62	RSSTGAVTTSNYAN	GTNNRVP	ALWYSNHWV
B2	VK4-1/JK5	98.32	KSSQSVLYRSNNKNCLT	WASTRES	QQYYSIPIT
B3	VK3-11/JK1	97.13	RASQSVRSYLV	DAFNRAT	QQRGNWPPT
B4	VK1-16/JK4	99.28	RASQGISNYLA	AASSLQS	QQYNSYPFT
B6	VK1-9/JK1	100	WASQGISSYLA	AASTLQS	QQLNSYPWT
B7	VL7-46/JL3	64.58	RSSTGAVTISNYAN	GTNNRVP	ALWYSNHWV
C4	VL4-69/JL1	72.11	TLSSQHSTYTIE	LKKDGSHSTGD	GVGDTIKEQFVYV
C7	VK3D-15/JK2	96.77	RASQSISSNVA	GSSTRAT	QQYHDWPS
D1	VK1-13/JK5	99.28	RASQGISSALA	DASSLES	QQFISYPIT
D4	VK1-17/JK4	98.92	RASQGIRNDLG	TASSLQS	LQHHSFPLT
D8	VK3-11/JK4	96.42	RASHSVSSYLA	DASNRAT	QQRSNWPLT
E2	VK1-6/JK1	100	RASQGIRNDLG	AASSLQS	LQDYNYPWT
E3	VK2-28/JK3	97.37	RSSQSLLYRNGYNYLE	LGSNRAS	MQTLQTPFT
E5	VK1-13/JK1	87.81	GASQGISNDLA	GASSRAS	QQDGSSPWT
E7	VK2-28/JK3	94.56	RSSQSLRYRNGYNYLD	EASNRAS	MQTVQTQFT
F3	VK4-1/JK4	98.32	KSSQSVLYSFKNKNYLA	WASTRES	QQYYSTPLT
F4	VK1-33/JK3	97.49	QASQDISNYLN	DASNVET	QQYDNLPFT
F6	VK3D-15/JK2	96.77	RASQSISSNVA	GASTRAT	QQYHDWPS
G4	VK2-28/JK3	96.26	RFSQSLLYRNGYNYLD	LGSNRAS	MQTLQTPFT
G7	VK1-33/JK3	97.85	QASQDISNYLN	DASNLET	QQYDNLPFT
H2	VK2-28/JK	97.37	RSSQSLLYRNGYNYLD	LGSNRAS	MQTLQTPFT
H3	VL7-46/JL3	64.93	RSSTGAVTTSNYAS	GTNNRVP	ALWYSNHWV
H4	VK2-28/JK3	97.62	RSSQSLLYRNGYNYLD	LGSNRAS	MQTLQTPFT

Fig. 1 (See legend on next page.)

(See figure on previous page.)

Fig. 1 Acquisition of mAbs secreted by single OMP-reactive B cells. **A** Schematic of HUGO-Ab mouse immunization. The initial dose of OMPs, combined with 50 μL of QuickAntibody Mouse3W, was administered via injection into the calf muscles of the HUGO-Ab mice. This was followed by two additional doses on days 14 and 21. The presence of anti-OMP antibodies was confirmed through ELISA following the third injection. Three days before testing with the Beacon system, each mouse received a final booster of OMPs via intraperitoneal injection. **B** The titer of OMP-specific polyclonal IgG antibodies at serial dilutions of 1:300, 1:2700, 1:24300 and 1:218700 in the serum obtained from immunized mice was assessed via ELISA. The values represent the means of triplicate technical replicate experiments, with SEMs indicated in the graph, and the significant differences in OMP-specific antibody levels compared with those in the non-immunized group are shown. **C** An 11k chip loaded with OMP-conjugated beads (left panel) or IgG beads (right panel), with a magnified view of a section to highlight the binding between the antibodies and beads over pens with OMP-reactive B cells or IgG-reactive B cells. **D** Germline, CDR1, CDR2, and CDR3 nucleotide sequences and variable region identities of the heavy or light chains of the recombinant mAbs were analyzed using the IMGT database. ***, $P < 0.001$; ****, $P < 0.0001$; unpaired Student's t test

plasma cell in the Nanopen secretes antibodies capable of binding to antigen microbeads, which exhibit a "bloom" phenomenon over time through their interactions with fluorescent secondary antibodies (Fig. 1C). Furthermore, IgG beads were loaded into individual NanoPens on the microfluidic chip to quantify the population of plasma cells that actively secrete antibodies (Fig. 1C). Statistical analysis revealed that among the 9021 plasma cells, 2029 secreted antibodies, of which 60 produced OMP-specific antibodies (Figure S2A). Therefore, we exported the 60 plasma cells for subsequent PCR amplification. Following single-cell isolation using the Beacon platform, PCR amplification was performed to amplify the light and heavy chain sequences from 60 individual cells (Figure S2B). Although technical difficulties were encountered during cDNA amplification of either the VH or VL genes from the extracted cellular material, paired VH and VL sequence information was successfully obtained and identified in 24 candidate cells. The Variable region amino acid sequences of the 24 candidates were obtained from the IMGT database (Table 2).

Using the IMGT database, a complementarity-determining region (CDR) analysis was performed, revealing that antibodies such as H2, H4, and E3 displayed highly homologous sequences in the CDRs of both VH and VL chains (Fig. 1D). Based on the similarities observed in the VH and VL CDRs among different mAbs, mAbs with distinct VH and VL CDRs were selected for further analysis, including B3, B4, B6, B7, C4, D4, D8, E2, E7, F2, F3, F4, F6, G7, and H2 (Fig. 1D). Subsequently, the identities of the variable regions and germline characteristics of VH and VL for these antibodies were analyzed, and 15 unique mAb sequences were identified. The VHs of B3, B4, B6, B7, C4, D4, D8, E2, E7, F2, F3, F4, F6, G7 and H2 were assigned to VH4-4/JH6/DH3-10,VH5-10-1/JH4/DH5-18,VH3-7/JH4/DH3-16,VH3-7/JH4/DH3-16,VH6-1/JH3/DH3-10,VH3-48/JH6/DH2-2,VH3-23/JH4/DH3-10,VH3-21/JH6/DH3-10,VH1-3/JH4/DH3-16,VH3-21/JH6/DH3-10,VH4-61/JH5DH2-2,VH6-1/JH6/DH5-12,VH3-20/JH6/DH1-14,VH6-1/JH6/DH5-12 and VH1-3/JH4/DH3-16 family, whereas their VL were categorized within VK3-11/JK1,VK1-16/JK4,VK1-9/JK1,VL7-46/JL3,VL4-69/JL1,VK1-17/JK4,VK3-11/JK4,VK1-6/JK1,VK2-28/JK3,VK1-6/JK1,VK4-1/JK4,VK1-33/JK3,VK3D-15/JK2,VK1-33/JK3 and VK2-28/JK family. Furthermore, with the exception of H2 VH (which exhibited 89.58% identity), the VHs demonstrated more than 90% identity in their variable regions compared to their respective germline genes (Fig. 1D). Among the 15 unique sequences of mAbs, we selected five sequences with VH and VL belonging to completely different families and high fluorescence intensity binding to Assay Beads on Beacon for expression. Specifically, fully human mAbs C4, F2, F3, F6, and G7 containing the human IgG1 constant region (IgG1 mAbs) and variable regions were expressed and purified (Figure S3).

Binding activity of Omp38-specific mAbs to *A. baumannii* strains

Among the outer membrane proteins (OMPs) of *A. baumannii*, Omp38 has been identified as a key factor in facilitating bacterial adhesion to and invasion of host cells [1, 19, 20]. We obtained the recombinant Omp38 as described in our previous study [22]. The results indicated that C4, F2, F3, F6, and G7 could bind to Omp38, with EC_{50} values ranging from 1.032 to 202.5 μg/mL (Fig. 2A). However, among the Omp38-specific fully human mAbs, only F2 was able to bind to the highly virulent strain LAC-4 of *A. baumannii*, with an EC_{50} value of 1.06 μg/mL (Fig. 2B). Further experiments revealed that F2 could also bind to LAC-4, ATCC 17,978, and clinical strains Strain1-ST193, Strain2-ST205, Strain3-ST2, and Strain6-ST63, indicating a certain degree of broad-spectrum binding (Fig. 2C).

Omp38-mAb F2 inhibited bacterial adherence and biofilm formation of *A. baumannii*

Epithelial cells serve as the initial barrier for immune defense in the host [28]. Biofilms formed by *A. baumannii* facilitate the attachment and colonization of the bacteria on respiratory epithelial cell surfaces, leading to their intracellular growth and eventual host cell death [19, 29]. Consequently, we investigated the effects of F2 on the pathogenicity of *A. baumannii*. Compared to the isotype control, F2 demonstrated inhibitory effects on both the adherence and biofilm formation of *A. baumannii* (Fig. 3A and B). Treatment with 100 μg/mL F2 reduced the mean $\log_{10}$CFU of *A. baumannii* adhering to

A549 cells from 7.56 to 6.65 (12.1% reduction) (Fig. 3A), which was comparable to that of murine mAb C3 (19.0% reduction) in our previous study (Figure S4A) [22]. Furthermore, F2 inhibited biofilm formation. At concentrations of 400, 200, 100, and 50 μg/mL, F2 reduced biofilm formation by 42.9%, 42.8%, 40.0%, and 22.3%, respectively (Fig. 3B). This inhibitory profile matched that of murine mAb C3 (51.9%, 46.7%, 42.2%, and 27.5%, respectively) at the same concentrations (Figure S4B) [22].

Analysis of the Omp38-mAb F2 binding conformation to explore the potential mechanism of the broad-spectrum binding activity of mAb F2

To investigate the binding epitope of mAb F2 to Omp38, predictions made using Alphafold3 and GeoBiologics indicated that mAb F2 might bind to the extracellular domain of Omp38 in the reference strain (ATG88079.1) (Fig. 4A). Further analysis of the binding conformation between F2 and Omp38 revealed that F2 bound to the four-loop structures in the extracellular regions of Omp38 (Fig. 4B). Subsequently, residues from the four loops of various *A. baumannii* strains, including the reference strain and the aforementioned nine clinical strains, were extracted and compared. We found that some strains of *A. baumannii*, such as clinical strains 2 and 6, possessed the same Omp38 loop structure; therefore, these strains were grouped for subsequent analyses (Fig. 4C). The nine strains were ultimately categorized into four groups, and four binding conformations were constructed based on homology modeling (Fig. 4C). Subsequently, we calculated the interaction energy of the four groups and found that mAb F2 exhibited the strongest binding affinity with Group1(strain3), with an interaction energy of −918.028 kcal/mol, followed by Group4 (strain8) at −846.226 kcal/mol (Fig. 4D). These findings were consistent with the ELISA results (Fig. 2C and D), supporting the reliability of the structural predictions.

Given the critical role of hydrogen bonds in achieving high specificity and affinity in antigen-antibody interactions [30, 31], the key hydrogen bonds involved in the interactions between the light chain, heavy chain, loop regions, and CDRs were annotated based on the 3D spatial structure of the reference strain (Fig. 4bonds between the antigen and mAb F2 A). After comparing the four binding conformations, we found that each loop structure of Omp38 contained several key amino acid residues, the side chains of which contributed to the formation of hydrogen bonds between the antigen and mAb F2 (Fig. 4E). Among the four binding conformations, several key residues were highly conserved, such as 37Q in loop1 (Fig. 4E). Although other critical residues varied across different strains, they still contributed essential hydrogen bonds for antibody binding. For example, when 71S in loop2 was mutated to 71Y, hydrogen bonds were still established between the hydroxyl group and the corresponding antibody residue (Fig. 4E). The preservation of this binding mode may explain the broad-spectrum activity of F2.

Omp38-mAb F2 did not confer protection against lethal *A. baumannii* infection in mice

To evaluate the protective efficacy of the fully human mAb F2 against highly virulent *A. baumannii* strain LAC-4, mice were intratracheally inoculated with a lethal dose of LAC-4 and subsequently administered Omp38-specific mAbs. Survival rates were monitored over a 72-hour postinfection period (Fig. 5A). However, the results demonstrated that mAb F2 failed to confer significant protection against lethal *A. baumannii* infection in a murine model (Fig. 5B).

Discussion

In this study, we isolated several mAbs targeting the OMPs of *A. baumannii* using a high-throughput screening approach on the Beacon platform. The variable regions of these mAbs were cloned into mammalian expression vectors containing constant human IgG1 regions to generate fully-human mAbs. Following the identification of Omp38-specific fully human mAbs, their binding activities were validated against *A. baumannii* strains from diverse sources. Finally, we investigated the potential mechanism underlying the broad-spectrum binding capability of mAb F2.

This study primarily focused on evaluating the protective efficacy of mAbs against *A. baumannii*. Subsequently, antimicrobial resistance profiling of clinical strains was performed exclusively through in silico analysis of second-generation sequencing data using the CARD database platform. Future investigations will incorporate phenotypic drug susceptibility testing, including Kirby-Bauer disk diffusion, broth microdilution, and E-test methodologies, to comprehensively characterize the multidrug-resistant (MDR) and extensively drug-resistant (XDR) profiles of these isolates. In the *A. baumannii* adherence and biofilm inhibition assays, we employed isotype controls (an irrelevant IgG mAb), as this approach is well-established in similar adhesion and biofilm studies to account for nonspecific binding and ensure the specificity of the observed effects [19]. However, we did not include a positive control mAb (e.g., a fully human mAb targeting *A. baumannii*) owing to the absence of successfully developed fully human mAbs.

In this study, the main reason for using LAC-4 instead of the thin capsule-forming *A. baumannii* ATCC 17,978 to establish the infection model is that our laboratory's current model for ATCC 17,978 is not yet mature. At the same bacterial concentration, *A. baumannii* ATCC 17,978 fails to cause mortality in mice, whereas the highly

Table 2 Complete amino acid sequences of the variable regions of the heavy and light chains of 24 candidate mAbs

Name	Variable region amino acid sequence
F2-H	QVQLVQSGAEVKKPGASVKVSCKASGYTFTRYVIHWVRQAPGQRLEWMGWINAGNGNTKYSEKFQGRVTITRDTSASTSYMELSSLRSEDTAVYYCARAGMD-VWGQGTTVTVSS
F2-L	DVVMTQSPLSLPVTLGQPASFSCRSSQSLVYSDGDTYLNWFQQRPGQSPRRLIYKVSNRDSGVPDRFSGSGSGTDFTLKISRVEAEDVGVYYCMQGTHWPLT-FGGGTKVEIK
A7-H	EVQLVESGGGLVQPGGSLRLSCAGSGFTFSTYWMSWVRQAPGKGLEWVANIKQDGSEKYYVDSVKGRFTISRDNANNSLYLQMNSLRAEDTAVYYCARGLIAY-WGQGTLVTVSS
A7-L	QAVVTQESALTTSPGETVTLTCRSSTGAVTTSNYANWVQEKPDHLFTGLIGGTNNRVPGVPARFSGSLIGDKAALTITGAQTEDEAIYFCALWYSNHWVFGGGT-KLTVL
B2-H	QVQLQESGPGLVKPSETLSLTCTVSGGSIRSSSNYWAWIRQPPGKGLEWIGSIYYSGSTYYNPSLKSRVTISVDTSKNQFSLKLSSVTAADTAVYYCARGGVRGVLN-WFDPWGQGTLVTVSS
B2-L	DIVMTQSPDSLALSLGERATINCKSSQSVLYRSNNKNCLTWYQQKPGQPPKVLIYWASTRESGVPDRFSGSGSGTDFTLTISSLQAEDVAVYYCQQYYSIPITFGQG-TRLEIK
B3-H	QVQLQESGPGLVKPSGTLSLTCSVSGGSISSSDWWSWVRQSPGKGLEWIGEIYHSGSTNYNPSLKSRVTISVDKSKNQFSLKLGSVTAADTAVYYCARS-GYYESGSFDYYHGLDVWGQGTTVTVSS
B3-L	EIVLTQSPATLSLSPGERATLSCRASQSVRSYLVWYQQRPGQALRLLIYDAFNRATGIPARFSGSGSGTDFTLTISSLEPEDFAVYYCQQRGNWPPTFGQGTKVEIR
B4-H	EVQLVQSGAEVKKPGESLRISCKGSGYSFTSYWISWVRQMPGKGLEWMGRIDPSDFYTNYSPSFQGHVTISADKSISTAYLQWSSLKASDTAMYYCARTRGYSDF-WGQGTLVTVSS
B4-L	DIQMTQSPSSLSASVGDRVTITCRASQGISNYLAWFQQKPGKAPKFLIYAASSLQSGVPSKFSGSGSGTDFTLTISSLQPEDFATYYCQQYNSYPFTFGGGTKVEIK
B6-H	EVQLVESGGGLVQPGGSLRLSCAASGFTFSTYWMSWVRQAPGKGLEWVANIKQDGSEKYYVDSVKGRFTISRDNANNSLYLQMNSLRAEDTAVYYCTRGLIAYW-GQGTLVTVSS
B6-L	DIQLTQSPSFLSASVGDRVTITCWASQGISSYLAWYQQKPGKAPKLLIYAASTLQSGVPSRFSGSGSGTEFTLTISSLQPEDFATYYCQQLNSYPWTFGQGTKVEIK
B7-H	EVQLVESGGGLVQPGGSLRLSCAASGFTFSTYWMSWVRQAPGKGLEWVANIKQDGSEKYYVDSVKGRFTISRDNAKNSLYLQMNSLRAEDTAVYYCARGLIAYW-GQGTLVTVSS
B7-L	QVAVTQESALTTSPGETVTLTCRSSTGAVTISNYANWVQEKPDHLFTGLIGGTNNRVPGVPARFSGSLIGDKAALTITGAQTEDEAIYFCALWYSNHWVFGGGT-KLTVL
C4-H	QVQLQQSGPGLVKPSQTLSLTCAISGDSVSSNSAAWSWIRQSPSRGLEWLGRTYYRSKWYNDYAVSVKSRISINPDTSKNQFSLQLNSVTPEDTAVYYCARLRITM-VRRIIIYDTFDIWGQGTMVTVSS
C4-L	QLVLTQSSSASFSLGASARLTCTLSSQHSTYTIEWYQQQPLKPPKYVMELKKDGSHSTGDGIPDRFSGSSSGADRYLSISNIQPEDEAIYICGVGD-TIKEQFVYVFGGGTKVTVL
C7-H	EVQLVESGGGVVRPGGSLRLSCAASGFTFDDYGMSWVRQVPGKGLEWVSGINWNGGSKGYVDSVKGRFTISRDNANSLYLQMDSLRVEDTAFYY-CARDRKRTHYYFKGLDVWGQGTTVTVSS
C7-L	EIVMTQSPATLSVSPGERPTLSCRASQSISSNVAWYQQKPGQAPRLLIYGSSTRATGIPARFSGSGSGTEFTLTISSLQSEDFAVYHCQQYHDWPSFGQGTRLEIK
D1-H	QVQLQQWGAGLLKPSETLSLTCAVDGGSFSGHYWSWIRQPPGKGLEWIGEINHSESTNYIPSLMSRVTISVDTSKNQFSLKLSSVTAADTAVYYCARGRVGATN-WFDPWGQGTLVTVSS
D1-L	AIQLTQSPSSLSASVGDRVTITCRASQGISSALAWYQQKPGKAPKLLIYDASSLESGVPSRFSGSGSGTDFTLTISSLQPEDFATYYCQQFISYPITFGQGTRLEIK
D4-H	EVQLVESGGGLVQSGGSLRLSCAASGFTFSSYSMNWVRQAPGKGLEWVSYISSSSSLIYYADSVKGRFTISRDNAKNSLYLQMNSLRDEDTAVYYCVPHMDVW-GQGTTVTVSS
D4-L	DIQMTQSPSSLSASVGDRVTITCRASQGIRNDLGWYQQKPGKAPKRLIYTASSLQSGVPSRFSGSGSGTEFSLTISSLQPEDFATYYCLQHHSFPLTFGGGTKVEIK
D8-H	EVQLVESGGGLVQPGGSLRLSCAASGFTFSSYAMRWVHQAPGKGLEWVSVISGSGTSTYSAVSVKGRFSISRDNSKITLYLQMNTLRAEDTAVYYCPKENGGFGE-LADFWGQGTLVTVSS
D8-L	EIVLSQSPASLSSSPGERVTLSCRASHSVSSYLAWYQQKPGQAPRLLIYDASNRATGIPSRFSGSGSGTDFTLTISSLEPEDFAVYYCQQRSNWPLTFGRGTKVEIK
E2-H	EVQLVESGGGLVKPGGSLRLSCAASGFTFSSYSMNWVRQAPGKGLEWVSSISSSSSYIYYADSVKGRFTISRDNAKNSLYLQMNSLRAEDTAVYY-CARNGYYYGSGSPYGMDVWGQGTTVTVSS
E2-L	AIQMTQSPSSLSASVGDRVTITCRASQGIRNDLGWYQQKPGKAPKLLIYAASSLQSGVPSRFSGSGSGTDFTLTISSLQPEDFATYYCLQDYNYPWTFGQGTKVEIK
E3-H	QVQLVQSGAEVKKPGASVKVSCKASGYTFTNYAIHWVRQAPGQRLEWMGWINAGKGNTEYSQKFQDRVTFTRDTSANTAYMELSSLRSEDTAVYYCTREG-DYVGGNYRPPFDYWGQGTLVTVSS
E3-L	DIVMTQSPLSLPVTPGEPASISCRSSQSLLYRNGYNYLEWYLQKSGHSPQLLIYLGSNRASGVPDRFSGSGSGTDFSLKISRVEAEDVGVYYCMQTLQTPFTFGPGT-KVAIK
E5-H	QVQLQQWGAGLLKPSETLSLTCAVYGGSFSGYYWSWIRQPPGKGLEWIGEINHSGSTNYNPSLKSRVTISVDTSRNQFSLKLSSVTAADTAVYYCARGPYYDILT-GYYYGMDVWDQGTTVTVAS
E5-L	TIQMTQSPSSLFASVGDRVIITGGASQGISNDLAWYQQKPGKAPKLLIYGASSRASGVPSRFSGSGSGTDFTLTISSLEPEDFAVYFCQQDGSSPWTFGQGTKVEIK
E7-H	QVQLVQSGAEVKKPGASVKVSCKASGYTFTSYAIHWVRQAPGQRLQWLGWINAGNGDTAYSQKFQGRVTITRDTSASTAYMDLSSLRSEDTALYYCTREGDYVW-GNYRPPFDYWGQGVLVTVSS
E7-L	DIAMTQSPLSLPVTPGEPASISCRSSQSLRYRNGYNYLDWYQQKPGQSPQLLIYEASNRASGVPDRFSGSGSGTDFTLKISRVEAEDVGIYYCMQTVQTQFTF-GQGTKVDIR
F3-H	QVQLQESGPGLVKPSETLSLTCTVSGGSVSSGRYYWSWIRQPPGKGLEWIGYIYYSGSTNYNPSLKSRVTISVDTSKNQFSLKLSSVTAADTAVYYCAREDCSSTNCY-ARWFDPWGQGTLVTVSS

Table 2 (continued)

Name	Variable region amino acid sequence
F3-L	DIVMTQSPDSLAVSLGERATINCKSSQSVLYSFKNKNYLAWYQQKRGQPPKLLIYWASTRESGVPDRFSGSGSGTDFTLTISSLQAGDVAVYYCQQYYSTPLT-FGGGTKVEIK
F4-H	QVQLQQSGPRLVKPSQTLSLTCAISGDSVASNSATWNWIRQSPSRGLEWLGRTYYRSKWNNDYAVSVKSRININPDTSKNQLSLQLNSVTPEDTAVYYCARGVATN-RGYRYYYEMDVWGQGTTVTVSS
F4-L	DIQLTQSPSSLSASVGDRVTITCQASQDISNYLNWYQQRPGKAPKVLIYDASNVETRVPSRFSGSGSGTDFTFTISSLQPEDFATYYCQQYDNLPFTFGPGTKVDIK
F6-H	EVQLVESGGGVVRPGGSLRLSCAASGFTFDDYGMSWVRQVPGKGLEWVSGINWNGGSKGYVDSVKGRFTISRDNAKNSLYLQMDSLRVEDTAFYY-CARDRKRTHYYFYGLDVWGQGTTVTVSS
F6-L	EIVMTQSPATLSASPGERPSLSCRASQSISSNVAWYQQKPGQAPRLLIYGASTRATGIPARFSGSGSGTEFTLTISSLQSEDFAVYHCQQYHDWPSFGQGTRLEIK
G4-H	QVQLVQSGAEVKKPGASVKVTCTASGYIFTSYAIHWVRQAPGQRLEWMGWINAGNGDTEYSHKFQGRVTITRDTFANTVYMELSSLRSEDTAVYFCTREGDYVW-GGYRPPFDYWGQGTLVTVSS
G4-L	DIVMSQSPLSLPVTPGEPASISCRFSQSLLYRNGYNYLDWYLQKPGQSPQVLIYLGSNRASGVPARFSGSGSGTDFTLKISRVEDEDVGVYYCMQTLQTPFTFGPGT-KVDIK
G7-H	QVQLQQSGPGLVKPSQTLSLTCAISGDIVSTNSATWNWIRQSPSRGLEWLGRTYYRSKWKNDYAVSVKSRVNIYPDTSKNQLSLQLNSVTPEDTAVYYCARGVATN-RGYQYFYEMDVWGQGTTVTVSS
G7-L	DIQLTQSPSSLSASVGDRVTITCQASQDISNYLNWYQQKPGKAPKVLIYDASNLETRVPSRFSGSGSGTDFTFTISSLQPEDFATYYCQQYDNLPFTFGPGTKVDIK
H2-H	QVQLVQSGAEVKKPGASVKVSCKASGYTFTNYAIHWVRQAPGQRLEWMGWINAGKGNTEYSQKFQDRVTFTRDTSANTAYMELSSLRSEDTAVYSCTREG-DYVGGNYRPPFDYWGQGTLVTVSS
H2-L	DIVMTQSPLSLPVTPGEPASISCRSSQSLLYRNGYNYLDWYLQKSGQSPQLLIYLGSNRASGVPDRFSGSGSGTDFSLKISRVEAEDVGVYYCMQTLQTPFTFGPGT-KVAIK
H3-H	EVHLVESGGGLVQPGGSLRLSCAASGLNFSTYWMSWVRQAPGKGLEWVANIKQDGSEKYYADSVKGRFTVSRDNAKNSLYLQMNSLRAEDTAVYYCTRGLIAY-WGQGTLVTVSS
H3-L	QAVVTQESALTTSPGETVSLTCRSSTGAVTTSNYASWVQERPDHLFTGLIGGTNNRVPGIPARFSGSLIGDKAALTITGAQTEDEAIYFCALWYSNHWVFGGGTKLTVL
H4-H	QVQLVQSGAEVKKPGASVKVSCKASGYTFTNYAIHWVRQAPGQRLEWMGWINAGKGNTEYSQKFQDRVTFTRDTSANTAYMELSSLRSEDTAVYSCTREG-DYVGGNYRPPFDYWGQGTLVTVSS
H4-L	DIVMTQSPLSLPVTPGEPASISCRSSQSLLYRNGYNYLDWYLQKSGQSPQLLIYLGSNRASGVPDRFSGSGSGTDFSLKISRVEAEDVGVYYCMQTLQTPFTFGPGT-KVAIK

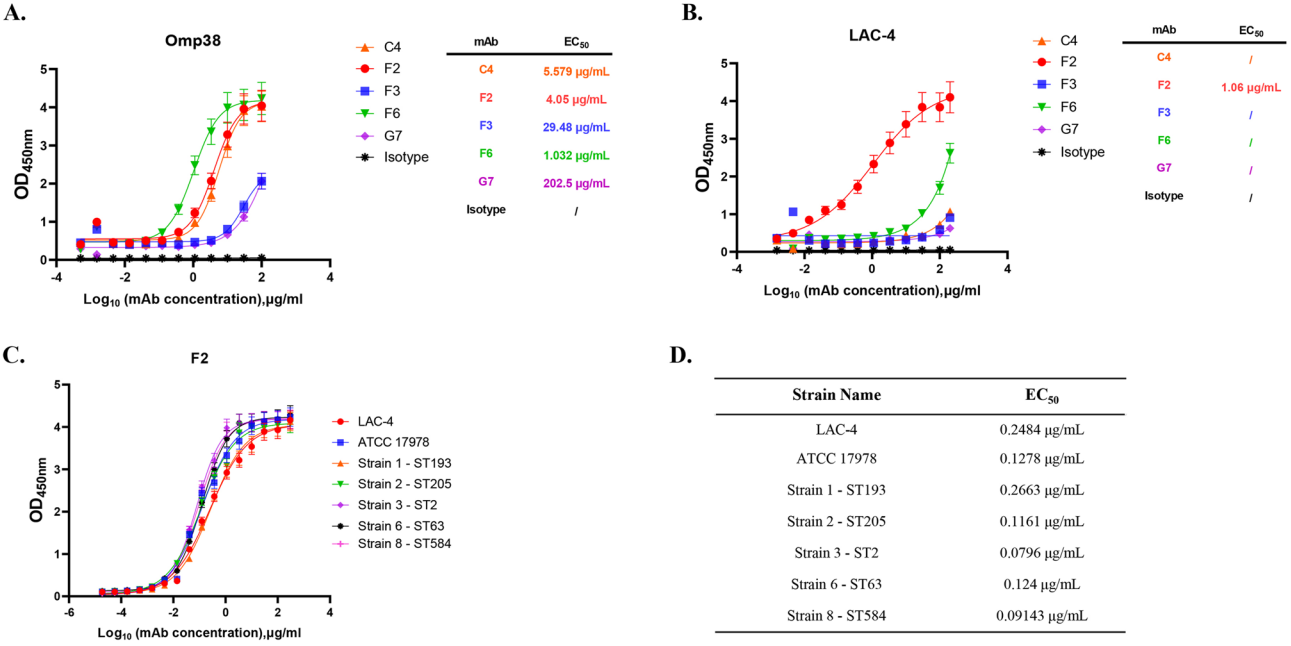

Fig. 2 Binding capacity of mAbs to Omp38 and *A. baumannii* strains. **A** ELISA assessment of the reactivities of the mAbs to Omp38. **B** Binding capacity of mAbs to *A. baumannii* strain LAC-4. **C** Binding activity of F2 to clinical *A. baumannii* strains. **D** EC_{50} of F2's binding activity to clinical *A. baumannii* strains. Curves were fitted using 4-parameter nonlinear regression. The means ± SEMs are shown, with $n = 3$ technical replicates

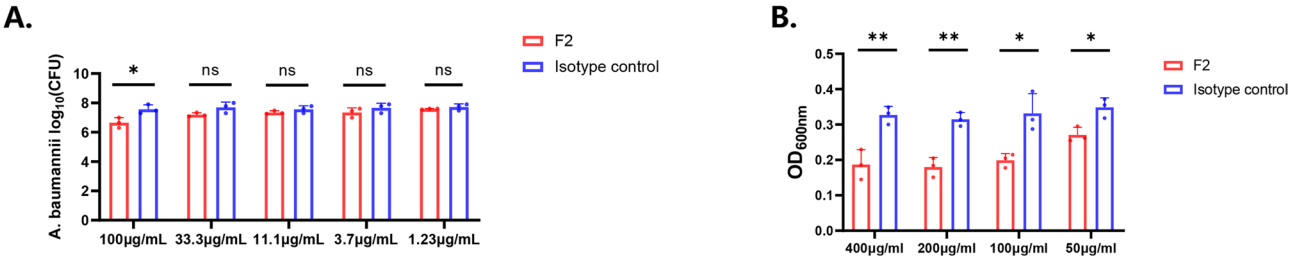

Fig. 3 mAb F2 inhibited bacterial adhesion and biofilm formation and induced antibacterial sterilization. **A** Adherence of *A. baumannii* ATCC 17,978 in the presence of the mAb F2 or the isotype control. **B** Biofilm formation by ATCC 17,978 in the presence of the mAb F2 or the isotype control. Each assay was performed in triplicate, and all the data are presented as the means ± SEMs from three independent experiments. Comparisons of bacterial loads between the groups were carried out via unpaired Student's t test. ns: not significant; *, $P < 0.05$; **, $P < 0.01$

virulent strain LAC-4 successfully induces lethal infection (Figure S1). Therefore, in subsequent studies, further optimization is needed to develop a suitable infection model for ATCC 17,978 that accurately reflects its pathogenic potential without confounding factors.

We also explored the protective effect of fully human mAbs against *A. baumannii* infection and found that F2 did not demonstrate protective effects in a lethal infection model. The main reasons for this phenomenon may be that the clearance of *A. baumannii* relies not only on the neutralizing ability of the Fab fragment of the antibody but also on the interaction of the Fc fragment with components of the immune system [32]. Because the Fc fragment of IgG-type antibodies has different affinities for various subtypes of FcγR [33], it is essential to consider the affinity of the humanized Fc fragment for mouse FcγR when conducting functional validation of fully human antibodies in mouse models. Gillian Dekkers and colleagues found that mouse and human FcγRs share approximately 60–70% homology, indicating that there may be incompatibility between the humanized Fc fragment of the antibody and mouse FcγR during functional validation in mouse models [32]. In addition, differences in receptor function and cellular expression patterns also contribute to incompatibility [33]. For example, human FcγRIIA contains an intracellular ITAM that is not present in the murine ortholog, and human FcγRIIA is not, but mouse FcγRIII is expressed on NK cells and mast cells [33]. Moreover, human FcγRIIC and FcγRIIIB is not present in mice [33]. To address this issue, some researchers have utilized humanized mouse models that lack endogenous FcγR but express human FcγR, and have encountered various challenges [32, 34]. Conventional strategies for generating fully humanized FcγR mice involve knocking out all murine activating FcγRs and crossing them with transgenic animals expressing the complete repertoire of human FcγRs [33, 35]. However, a key challenge in this approach lies in maintaining multiple transgenes in an FcγR-deficient murine background, which demands considerable technical expertise and careful genetic management. Another approach for generating fully humanized FcγR mice involves engrafting immunodeficient mice with a human immune system comprising all hematopoietic cell lineages [33, 36]. However, this model presents several limitations. First, both murine and human effector cells expressing species-specific FcγRs coexist in the peritoneal cavity, potentially competing for engagement by human IgG1 [33]. Moreover, human cells fail to properly repopulate key immunological niches like bone marrow, resulting in only transient reconstitution [33]. Therefore, future investigations should employ larger mammalian models, such as rhesus monkeys, which exhibit FcγR expression profiles closely resembling those of humans, to more accurately evaluate the therapeutic efficacy of fully human mAbs. In subsequent studies, we aim to further elucidate the molecular mechanisms underlying the protective effects of mAbs using more physiologically relevant animal models. First, utilizing Fc receptor knockout humanized mice models, we will systematically validate whether the protective efficacy of mAbs depends on the specific interaction between their Fc region and Fc receptors. Second, fluorescence or radiolabeling techniques will be employed to conduct biodistribution studies of mAbs, aiming to elucidate their tissue distribution profiles in animal models, particularly their targeted enrichment capability at infection sites. Concurrently, pharmacokinetic experiments will be performed to evaluate key pharmacological parameters such as half-life, clearance rate, and bioavailability of mAbs in vivo, thereby providing a pharmacokinetic basis for their protective effects.

In this study, adhesion and biofilm formation assays were conducted using *A. baumannii* strain ATCC 17,978 (thin capsule), whereas animal challenge experiments employed the hypervirulent strain LAC-4 (thick capsule). Previous study showed that dense capsules may physically block mAbs from accessing outer membrane proteins such as Omp38 [37]. The observed lack of in vivo efficacy in the LAC-4 lethal infection model may thus be attributed to reduced accessibility of mAb F2 to Omp38 caused by LAC-4's thick capsule. To elucidate the underlying mechanism, further structural investigations

A.

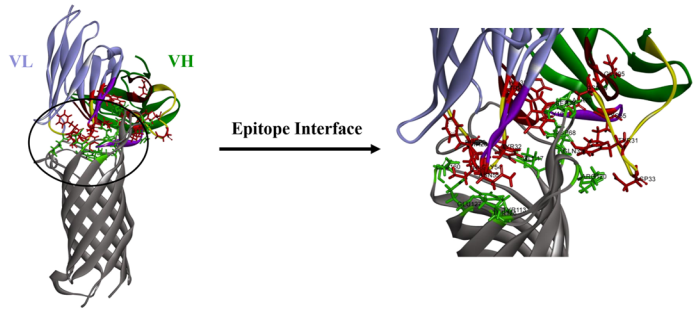

CDR	mAb	OMP ref	Type
	THR28	GLU160	Hydrogen bond
	PHE29	GLU160	Hydrogen bond
	THR30	GLU160	Hydrogen bond
HCDR1		TYR113	Hydrogen bond
		GLU127	Hydrogen bond
	TYR32	GLN17	Hydrogen bond
	HIS35	SER71	Hydrogen bond
	TRP50	SER71	Hydrogen bond
HCDR2	GLY54	GLU127	Hydrogen bond
	ASN55	ASP68	Hydrogen bond
		THR125	Hydrogen bond
HCDR3	GLY100	ASP68	Hydrogen bond
	TYR31	ARG120	Hydrogen bond
LCDR1	ASP33	ARG120	Salt Bridge
	ASN39	GLN37	Hydrogen bond
LCDR2	LYS55	ASP68	Hydrogen bond
LCDR3	GLY96	ALA70	Hydrogen bond

B.

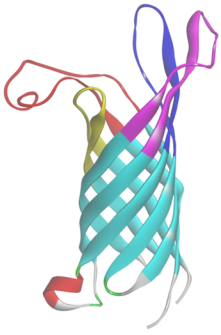

Loop Name	Amino Sequence
Loop1	YTFQDSQHNNGGKDGN LTNSPELQDDL
Loop2	NQVKGDVDGASAGAEY KQKQ
Loop3	HYKYDFDGVNRGTRGTS EEGT
Loop4	ARATYNADEEFWNYTA

C.

Loop1	
Reference Strain	YTFQDSQHNNGGKDGNLTNSPELQDDL
Strian1	YTFQDSQHNNGGKDGSLTNGPELQDDL
Strian2	YTFQDSQHNNGGDKGELTNGPELQDDL
Strain3	YTFQDSQHNNGGKDGNLTNSPELQDDL
Strain4	YTFQDSQHNNGGKDGNLTNSPELQDDL
Strain5	YTFQDSQHNNGGKDGNLTNSPELQDDL
Strain6	YTFQDSQHNNGGDKGELTNGPELQDDL
Strain7	YTFQDSQHNNGGKDGNLTNSPELQDDL
Strain8	YTFQDSEHNN----HKLTDSPELQDDL
Strain9	YTFQDSQHNNGGKDGNLTNSPELQDDL

Loop3	
Reference Strain	HYKYDFDGVNRGTRGTSEEGT
Strain1	HYKYDFDDARLAYHDG-EEGT
Strian2	HYKYEFDDARLAYHDG-EEGT
Strain3	HYKYDFDGVNRGTRGTSEEGT
Strain4	HYKYDFDGVNRGTRGTSEEGT
Strain5	HYKYDFDGVNRGTRGTSEEGT
Strain6	HYKYEFDDARLAYHDG-EEGT
Strain7	HYKYDFDGVNRGTRGTSEEGT
Strain8	HYKYDFDDARLAYHDG-EEGT
Strain9	HYKYDFDGVNRGTRGTSEEGT

Loop2	
Reference Strain	NQVKGDVDGASAGAEYKQKQ
Strain1	NQVKGDVDTNYG---EYKQKQ
Strian2	NQVKGDVDPNYG---EYKQKQ
Strain3	NQVKGDVDGASAGAEYKQKQ
Strain4	NQVKGDVDGASAGAEYKQKQ
Strain5	NQVKGDVDGASAGAEYKQKQ
Strain6	NQVKGDVDPNYG---EYKQKQ
Strain7	NQVKGDVDGASAGAEYKQKQ
Strain8	NQVKGDVDPNYG---EYKQKQ
Strain9	NQVKGDVDGASAGAEYKQKQ

Loop4	
Reference Strain	ARATYNADEEFWNYTA
Strain1	ARGTYNFDEQFWNYTA
Strian2	ARGTYNFDEKFWNYTA
Strain3	ARATYNADEEFWNYTA
Strain4	ARATYNADEEFWNYTA
Strain5	ARATYNADEEFWNYTA
Strain6	ARGTYNFDEKFWNYTA
Strain7	ARATYNADEEFWNYTA
Strain8	ARGTYNFDEKFWNYTA
Strain9	ARATYNADEEFWNYTA

D.

Group	Antigen Name	Interaction energy with C3 (kcal/mol)
1	Reference strain, Strain3, Strain4, Strain5, Strain7, Strain9	-918.026
2	Strain1	-783.768
3	Strain2, Strain6	-791.695
4	Strain8	-846.226

E.

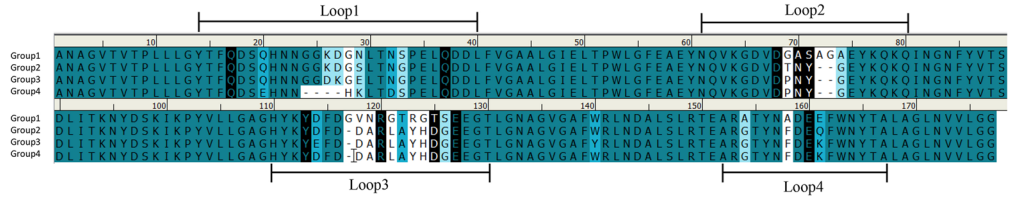

Fig. 4 Predicted interaction between mAb F2 and *A. baumannii*. **A** Predicted binding between mAb F2 and the *A. baumannii* reference strain modeled by AlphaFold 3 and GeoBiologics. **B** The four loop regions of the Omp38 extracellular domain predicted by Discovery Studio 2.5. Loop 1, loop 2 and loop 3 are shown in red, blue, pink, and yellow, respectively. **C** Alignment of the loop region sequences from different strains on the basis of 3D structure by Discovery Studio 2.5 (Accelrys Software, Inc.) The same structure is displayed in the same color. **D** The interaction energy between F2 and different strains of *A. baumannii* was calculated using CHARMm with the tools implemented in Discovery Studio 2.5 (Accelrys Software, Inc.). **E** Identification of the key residues in the four binding conformations by Discovery Studio 2.5 (Accelrys Software, Inc.). The key residues are shown in red. Group 1: reference strain, strain 3, strain 4, strain 5, strain 7, and strain 9. Group 2: strain 1. Group 3: strain 2 and train 6. Group 4: strain 8

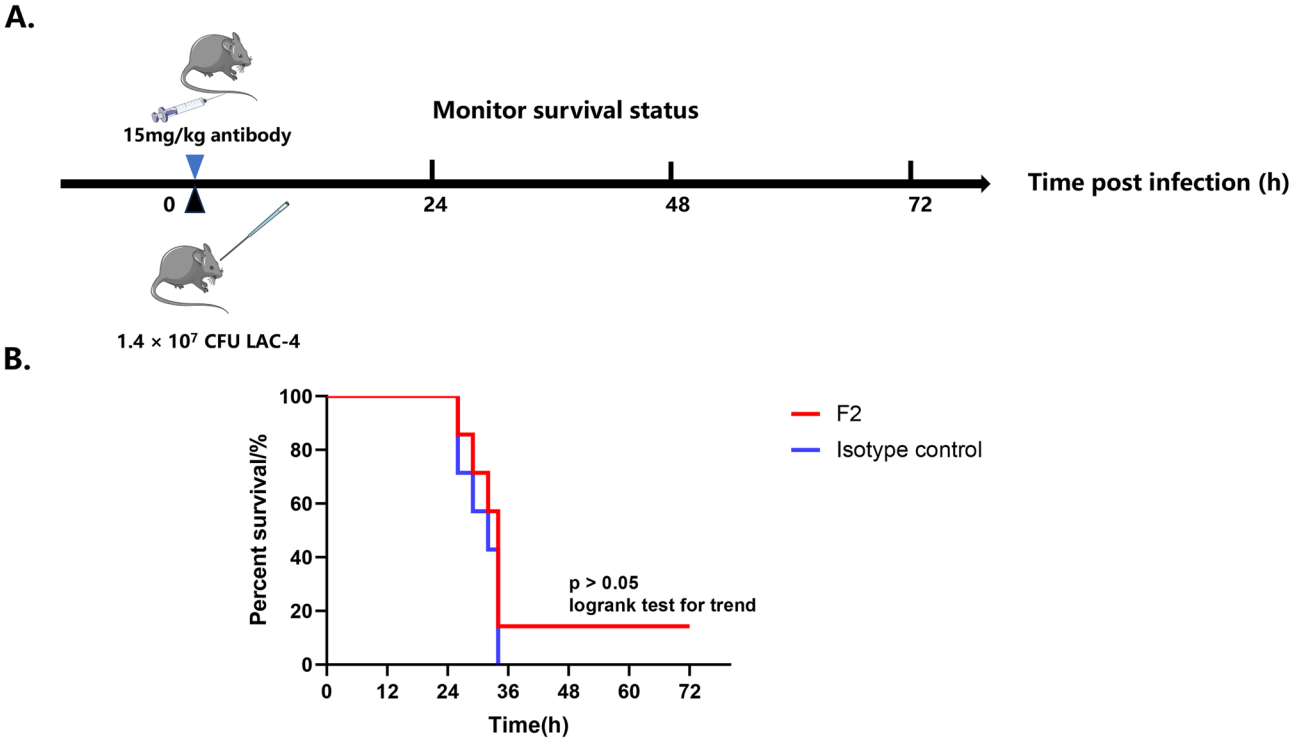

Fig. 5 Impact of IgG1 mAbs in a lethal LAC-4 infection model. **A** Diagram illustrating the treatment of model mice with lethal LAC-4 infection using Omp38-specific mAbs. Seven mice were non-invasively intratracheally inoculated with a lethal dose (1.4×10^7 CFU) of LAC-4 and immediately administered 15 mg/kg of mAb F2 or an isotype control. The survival status of the mice was monitored for 72 h post-infection. **B** Kaplan–Meier survival curves comparing infected mice treated with a single mAb or a combination of mAbs versus isotype controls ($n=7$ per group, biological replicates). Survival curves were analyzed using the log-rank (Mantel–Cox) test. h: hours

would be informative, such as cryo-electron microscopy (cryo-EM) mapping of the interaction between mAb F2, Omp38, and the capsular matrix. *A. baumannii* biofilm formation occurs in three stages: (1) initial adhesion, (2) early development and (3) mature biofilm [38]. In this study, we focused on evaluating the mAb's activity against the first two stages but did not assess its efficacy against mature biofilms. Currently, strategies to disperse mature biofilms primarily involve natural compounds (e.g., honokiol and magnolol), synthetic agents (e.g., N-acetylcysteine), and antimicrobial peptides (e.g., magainin 2), with limited research on mAb-based approaches [38]. Future studies will include assays to examine the mAb's effects on mature biofilms, offering a more complete assessment of its therapeutic potential.

Antibody-dependent cellular phagocytosis (ADCP) represents a crucial immune defense mechanism in which mAbs specifically recognize and bind to infected cells, facilitating their engulfment and removal by phagocytic cells, particularly macrophages [39]. Research has confirmed the important role of macrophages in the initial stages of host immune response against *A. baumannii* infection, primarily through their capacity to effectively phagocytose and eliminate *A. baumannii* [40]. In this study, we did not validate whether F2 could mediate ADCP. The absence of ADCP data leaves an important aspect of Fc-mediated effector functions unexplored, which could theoretically contribute to F2's overall antibacterial efficacy through enhanced pathogen clearance. To address this limitation, we propose several experimental approaches in future studies. Enriching monocytes from human peripheral blood using magnetic beads, differentiating them into macrophages, and activating them prior to experimentation is a potential alternative. However, this approach requires substantial amounts of peripheral blood to obtain a sufficient number of macrophages for experimental needs. Alternatively, utilizing human macrophage cell lines (such as THP-1) for related experiments offers another potential solution [18], which represents an important method for further study. Furthermore, to comprehensively evaluate F2's interaction with immune cells, we will perform immune cell depletion studies, including neutrophil depletion via anti-Ly6G antibody pretreatment to assess whether F2's efficacy is diminished; macrophage depletion using clodronate liposomes to evaluate the impact on bacterial clearance; and NK cell depletion via anti-NK1.1 antibody treatment to examine its influence on antibody-dependent cellular cytotoxicity (ADCC).

In recent years, with the rapid advancement of artificial intelligence (AI) technologies, numerous computational models have been successfully applied to epitope prediction, including AlphaFold3, GeoBiologics, Bcepred, ABCpred, Discotope, BepiPred, and CEP [41, 42]. In this study, we employed bioinformatics analysis to investigate the binding epitope of the mAb F2, providing preliminary insights into the molecular mechanism underlying its broad-spectrum binding activity. Current epitope-validation methods (ELISA, enzymatic/chemical cleavage, alanine scanning, phage display, X-ray crystallography) have limitations for identifying the conformational epitope of mAb F2 binding to Omp38. ELISA lacks resolution for conformational epitopes; cleavage methods only detect linear epitopes; alanine scanning is labor-intensive and disrupts protein structure; phage display yields short, non-native peptides; and crystallography is impractical for Omp38's transmembrane structure. Instead, hydrogen/deuterium exchange mass spectrometry (HDX-MS) is ideal, offering high-resolution conformational analysis without crystallization and lower sample purity requirements [43, 44]. Thus, HDX-MS will be employed to experimentally map the mAb F2-Omp38 epitope.

Species specificity of the Omp38 protein is a critical consideration in antibody safety evaluation. Current studies indicate that Omp38 is not a species-specific protein of *A. baumannii* but exhibits structural homology with *Escherichia coli (E. coli)* Omp38 and *Pseudomonas aeruginosa (P. aeruginosa)* OprF, suggesting a potential risk of cross-reactive immune responses. To comprehensively assess antibody specificity, subsequent investigations will employ standardized methodologies, including ELISA and flow cytometry, to systematically evaluate cross-reactivity of candidate antibodies. Should cross-reactivity be detected, antibody engineering techniques—such as CDR mutagenesis or affinity maturation—will be implemented to enhance specificity. Based on these findings, the clinical application scope will be strictly defined (e.g., restricted to respiratory specimen testing while excluding intestinal samples to mitigate potential cross-reactivity).

Conclusions

In summary, our study successfully identified mAbs targeting OMPs using a high-throughput screening approach. Subsequently, we developed Omp38-specifc fully human mAb F2 and found that F2 potently and broadly bound to *A. baumannii* strains. Besides, F2 inhibited the bacterial adherence and biofilm formation of *A. baumannii*. Finally, we explore the potential mechanism of the broad-spectrum binding activity of mAb F2. Further research and development of F2 might pave the way for novel treatments, ultimately contributing to better management and control of *A. baumannii* infections in clinical settings.

Abbreviations

A. baumannii	*Acinetobacter baumannii*
ADCC	Antibody-dependent cellular cytotoxicity
ADCP	Antibody-dependent cellular phagocytosis
AI	Artificial intelligence
CARD	ComprehensiveAntimicrobial Resistance Database
CDR	Complementarity-determining region
CFUs	Colony-forming units
cryo-EM	Cryo-electron microscopy
E. coli	*Escherichia coli*
ELISA	Enzyme-linked immunosorbent assay
FBS	Fetal bovine serum
HAMA	Human anti-mouse antibody
HDX-MS	Hydrogen/deuterium exchange mass spectrometry
HRP	Horseradish peroxidase
HUGO-Ab	Humanized genomic orthologs for antibody development
ICUs	Intensive care units
mAbs	Monoclonal antibodies
MDR	Multidrug-resistant
OEP	OptoElectroPositioning
OMP	Outer membrane protein
P. aeruginosa	*Pseudomonas aeruginosa*
PBS	Phosphate-buffered saline
ps	Picosecond
RMS	Root-mean-square
SEMs	Standard errors of the means
ST	Sequence type
SPF	Specific pathogen-free
XDR	Extensively drug-resistant

Supplementary Information

The online version contains supplementary material available at https://doi.org/10.1186/s12866-025-04283-y.

Supplementary Material 1: Figure S1. Determination of optimal challenge dose in LAC-4 or ATCC 17978 infection model. Mice were infected with varying dose of LAC-4 or ATCC 17978 (1.2×10^7, 1.4×10^7,1.6×10^7, or 1.8×10^7 CFU), and survival rate was monitored over 72 hours (n = 6 per group, biological replicates). The 1.2×10^7 CFU dose of LAC-4 induced sublethal infection (66.7% mortality), while 1.6×10^7 CFU and 1.8×10^7 CFU caused rapid lethality (<30h), precluding therapeutic evaluation. The intermediate dose of LAC-4 (1.4×10^7 CFU) achieved consistent 100% mortality within 72 hours while permitting a sufficient window for intervention studies. However, ATCC 17978 could not induce the death of mice within 72 hours at the same concentration. h: hours.

Supplementary Material 2: Figure S2. Identification of OMP-specific mAbs via the Beacon platform. (A) A concise summary of functional assays, highlighting the total cell count in the NanoPens (Pen Number), the number of cells producing antibodies (IgG-Reactive Number), and the number of cells secreting antibodies reactive to OMP (OMP-Reactive Number). (B) PCR amplification products for the antibody heavy chain (upper panel) and light chain (lower panel) derived from single B cells.

Supplementary Material 3: Figure S3. Expression and validation of the purified IgG1 mAbs. (A) Non-reducing PAGE analysis showed that the mAbs migrated at around 150 kDa. In contrast, reducing PAGE demonstrated that the mAb heavy chain migrated at approximately 55 kDa, while the light chain migrated at about 25 kDa. Ipilimumab (IPI) served as a positive control. (B) SEC-HPLC was employed to achieve highly sensitive detection of the expressed mAbs.

Supplementary Material 4: Figure S4. Comparison of the inhibitory effects of fully human mAb F2 and murine mAb C3. (A) Comparison of the inhibitory effects of fully human mAb F2 and murine mAb C3 on ***A. baumannii*** adherence. (B) Comparison of the inhibitory effects of fully human mAb F2 and murine mAb C3 on ***A. baumannii*** biofilm formation. Each assay was performed in triplicate, and all the data are presented as the means ±

SEMs from three independent experiments. Comparisons of percentage reduction between the groups were carried out via unpaired Student's t test. ns: not significant.

Acknowledgements
We acknowledge the technical support provided by Di Yang, Jian Zhou and Jingxue Wang (Institute of Immunology, Third Military Medical University (Army Medical University), Chongqing 400038, People's Republic of China) for their assistance with animal experiments. We also extend our gratitude to Chao Han (Institute of Immunology, Third Military Medical University (Army Medical University), Chongqing 400038, People's Republic of China) and Shuai Xu (The Second Affiliated Hospital, Third Military Medical University (Army Medical University), Chongqing 400037, People's Republic of China) for their valuable input and discussions. Finally, we thank all members of our laboratory for their constructive feedback and support throughout this study.

Authors' contributions
Y.-W.Z.: Writing – original draft, Investigation. W.-K.Y.: Writing – original draft, Investigation. P.Y.: Methodology, Supervision, Conceptualization. S.-F.W.: Methodology, Supervision, Software. H.D.: Methodology, Validation. Y.Q.: Methodology, Resources. X.-H.C.: Methodology, Resources. L.Z.: Methodology, Data curation. Y.-X.L.: Methodology, Data curation. X.M.: Methodology, Data curation. T.-T.Z.: Investigation, Methodology. J.-B.Z.: Resources. X.-M.C.: Investigation, Methodology. H.-B.L.: Writing – review & editing, Project administration, Conceptualization. S.Z.: Methodology, Validation. Y.-Z.W.: Writing–review & editing, Project administration, Conceptualization. Y.T.: Writing–review & editing, Project administration, Funding acquisition, Conceptualization. All the authors reviewed and approved the final version of the manuscript.

Funding
This work was supported by grants from the General Program of the National Natural Science Foundation of China (no. 32170887 and No. 31970885), the Special Program of the National Natural Science Foundation of China (no. 32141005), and the Major Research Plan of the National Natural Science Foundation of China (no. 92269110). Special fund for performance incentive guidance of research institutions in Chongqing (cstc2021jxjl130036) and Chongqing International Institute for Immunology Project (2022YJC01). The funders had no role in the study design, data analyses, or decision to publish.

Data availability
The datasets generated and analyzed during the current study, including the sequences of bacterial strains and mAbs, are available from the corresponding author upon reasonable request. The materials used in this study, such as cell lines and reagents, are commercially available or can be provided by the authors under appropriate agreements.

Declarations

Ethics approval and consent to participate
All experimental procedures involving animals were conducted in strict accordance with the guidelines for the care and use of laboratory animals and were approved by the Animal Ethics and Experimental Committee of Army Medical University in Chongqing, China (Approval No. 20250017). Efforts were made to minimize animal suffering and to reduce the number of animals used in the study.

Consent for publication
Not applicable.

Competing interests
The authors declare no competing interests.

Author details
[1]Institute of Immunology, Third Military Medical University (Army Medical University, Chongqing 400038, People's Republic of China
[2]Department of Microbiology and Biochemical Pharmacy, National Engineering Research Center of Immunological Products, College of Pharmacy, Third Military Medical University (Army Medical University), Chongqing 400038, People's Republic of China
[3]Chongqing International Institute for Immunology, Chongqing 400030, People's Republic of China
[4]General Hospital of Central Theater Command, Wuhan 430070, Hubei, People's Republic of China
[5]Wuhan No.1 Hospital, Wuhan 430070, Hubei, People's Republic of China
[6]Cyagen Biosciences, 19 Dongcang South Road, Taicang, Jiangsu 215400, People's Republic of China
[7]The Second Affiliated Hospital, Third Military Medical University (Army Medical University, Chongqing 400037, People's Republic of China
[8]Department of Nephrology, Chinese PLA General Hospital, Chinese PLA Institute of Nephrology, National Key Laboratory of Kidney Diseases, National Clinical Research Center for Kidney Diseases, Beijing 100853, People's Republic of China

Received: 25 February 2025 / Accepted: 29 July 2025
Published online: 20 August 2025

References

1. Uppalapati SR, Sett A, Pathania R. The outer membrane proteins ompa, caro, and OprD of acinetobacter baumannii confer a Two-Pronged defense in facilitating its success as a potent human pathogen. Front Microbiol. 2020;11:589234. https://doi.org/10.3389/fmicb.2020.589234.
2. Zhou H, Yao Y, Zhu B, Ren D, Yang Q, Fu Y, et al. Risk factors for acquisition and mortality of multidrug-resistant acinetobacter baumannii bacteremia: A retrospective study from a Chinese hospital. Med (Baltim). 2019;98(13):e14937. https://doi.org/10.1097/md.0000000000014937.
3. Garnacho-Montero J, Dimopoulos G, Poulakou G, Akova M, Cisneros JM, De Waele J, et al. Task force on management and prevention of acinetobacter baumannii infections in the ICU. Intensive Care Med. 2015;41(12):2057–75. https://doi.org/10.1007/s00134-015-4079-4.
4. Dijkshoorn L, Nemec A, Seifert H. An increasing threat in hospitals: multidrug-resistant acinetobacter baumannii. Nat Rev Microbiol. 2007;5(12):939–51. https://doi.org/10.1038/nrmicro1789.
5. McConnell MJ. Where are we with monoclonal antibodies for multidrug-resistant infections? Drug Discov Today. 2019;24(5):1132–8. https://doi.org/10.1016/j.drudis.2019.03.002.
6. Haraya K, Tachibana T, Igawa T. Improvement of Pharmacokinetic properties of therapeutic antibodies by antibody engineering. Drug Metab Pharmacokinet. 2019;34(1):25–41. https://doi.org/10.1016/j.dmpk.2018.10.003.
7. Almagro JC, Daniels-Wells TR, Perez-Tapia SM, Penichet ML. Progress and challenges in the design and clinical development of antibodies for cancer therapy. Front Immunol. 2017;8:1751. https://doi.org/10.3389/fimmu.2017.01751.
8. Kohler G, Milstein C. Continuous cultures of fused cells secreting antibody of predefined specificity. Nature. 1975;256(5517):495–7. https://doi.org/10.1038/256495a0.
9. Litzow MR. Monoclonal antibody-based therapies in the treatment of acute lymphoblastic leukemia. Am Soc Clin Oncol Educ Book. 2013;294–9. https://doi.org/10.14694/EdBook_AM.2013.33.294.
10. Harding FA, Stickler MM, Razo J, DuBridge RB. The immunogenicity of humanized and fully human antibodies: residual immunogenicity resides in the CDR regions. MAbs. 2010;2(3):256–65. https://doi.org/10.4161/mabs.2.3.11641.
11. Davda J, Declerck P, Hu-Lieskovan S, Hickling TP, Jacobs IA, Chou J, et al. Immunogenicity of immunomodulatory, antibody-based, oncology therapeutics. J Immunother Cancer. 2019;7(1):105. https://doi.org/10.1186/s40425-019-0586-0.
12. Geiss R, De La Motte Rouge T, Dubot C, Leary A, Lhomme C, Pautier P, et al. [Targeted therapy in locally and metastatic recurrent cervical cancers]. Bull Cancer. 2014;101(7–8):748–55. https://doi.org/10.1684/bdc.2014.1949.
13. Singh S, Kumar NK, Dwiwedi P, Charan J, Kaur R, Sidhu P, et al. Monoclonal antibodies: A review. Curr Clin Pharmacol. 2018;13(2):85–99. https://doi.org/10.2174/1574884712666170809124728.
14. Safdari Y, Farajnia S, Asgharzadeh M, Khalili M. Antibody humanization methods - a review and update. Biotechnol Genet Eng Rev. 2013;29:175–86. https://doi.org/10.1080/02648725.2013.801235.
15. Tomszak F, Weber S, Zantow J, Schirrmann T, Hust M, Frenzel A. Selection of Recombinant human antibodies. Adv Exp Med Biol. 2016;917:23–54. https://doi.org/10.1007/978-3-319-32805-8_3.

16. Zou Y, Xu W, Li J. Chimeric antigen receptor-modified T cell therapy in chronic lymphocytic leukemia. J Hematol Oncol. 2018;11(1):130. https://doi.org/10.1186/s13045-018-0676-3.
17. Richardson E, Binter S, Kosmac M, Ghraichy M, von Niederhausern V, Kovaltsuk A, et al. Characterisation of the immune repertoire of a humanised Transgenic mouse through immunophenotyping and high-throughput sequencing. Elife. 2023;12. https://doi.org/10.7554/eLife.81629.
18. Baker S, Krishna A, Higham S, Naydenova P, O'Leary S, Scott JB, et al. Exploiting human immune repertoire Transgenic mice for protective monoclonal antibodies against antimicrobial resistant acinetobacter baumannii. Nat Commun. 2024;15(1):7979. https://doi.org/10.1038/s41467-024-52357-8.
19. Barati H, Fekrirad Z, Jalali Nadoushan M, Rasooli I. Anti-OmpA antibodies as potential inhibitors of acinetobacter baumannii biofilm formation, adherence to, and proliferation in A549 human alveolar epithelial cells. Microb Pathog. 2024;186:106473. https://doi.org/10.1016/j.micpath.2023.106473.
20. Zhang MN, Zhao XO, Cui Q, Zhu DM, Wisal MA, Yu HD, et al. Famotidine enhances rifampicin activity against acinetobacter baumannii by affecting OmpA. J Bacteriol. 2023;205(8):e0018723. https://doi.org/10.1128/jb.00187-23.
21. Li Y, Peng C, Zhao D, Liu L, Guo B, Shi M, et al. Outer membrane protein A inhibits the degradation of caspase-1 to regulate NLRP3 inflammasome activation and exacerbate the acinetobacter baumannii pulmonary inflammation. Microb Pathog. 2021;153:104788. https://doi.org/10.1016/j.micpath.2021.104788.
22. Zhang Y, Cheng H, Yu P, Wang S, Dong H, Lu S, et al. High-throughput single-cell analysis reveals Omp38-specific monoclonal antibodies that protect against acinetobacter baumannii infection. Emerg Microbes Infect. 2025;14(1):2437243. https://doi.org/10.1080/22221751.2024.2437243.
23. Yu P, Ran J, Yang R, Zhu H, Lu S, Wu Y, et al. Rapid isolation of pan-neutralizing antibodies against Omicron variants from convalescent individuals infected with SARS-CoV-2. Front Immunol. 2024;15:1374913. https://doi.org/10.3389/fimmu.2024.1374913.
24. Nguyen DC, Garimalla S, Xiao H, Kyu S, Albizua I, Galipeau J, et al. Factors of the bone marrow microniche that support human plasma cell survival and Immunoglobulin secretion. Nat Commun. 2018;9(1):3698. https://doi.org/10.1038/s41467-018-05853-7.
25. Hatefi Oskuei R, Darvish Alipour Astaneh S, Rasooli I. A conserved region of acinetobacter trimeric autotransporter adhesion, ata, provokes suppression of acinetobacter baumannii virulence. Arch Microbiol. 2021;203(6):3483–93. https://doi.org/10.1007/s00203-021-02343-1.
26. Li S, Chen DQ, Ji L, Sun S, Jin Z, Jin ZL, et al. Development of different methods for Preparing acinetobacter baumannii outer membrane vesicles vaccine: impact of Preparation method on protective efficacy. Front Immunol. 2020;11:1069. https://doi.org/10.3389/fimmu.2020.01069.
27. Gu H, Liu D, Zeng X, Peng LS, Yuan Y, Chen ZF, et al. Aging exacerbates mortality of acinetobacter baumannii pneumonia and reduces the efficacies of antibiotics and vaccine. Aging. 2018;10(7):1597–608. https://doi.org/10.18632/aging.101495.
28. Bergman P, Raqib R, Rekha RS, Agerberth B, Gudmundsson GH. Host directed therapy against infection by boosting innate immunity. Front Immunol. 2020;11:1209. https://doi.org/10.3389/fimmu.2020.01209.
29. Zarrilli R. Acinetobacter baumannii virulence determinants involved in biofilm growth and adherence to host epithelial cells. Virulence. 2016;7(4):367–8. https://doi.org/10.1080/21505594.2016.1150405.
30. Madsen AV, Mejias-Gomez O, Pedersen LE, Preben Morth J, Kristensen P, Jenkins TP, et al. Structural trends in antibody-antigen binding interfaces: a computational analysis of 1833 experimentally determined 3D structures. Comput Struct Biotechnol J. 2024;23:199–211. https://doi.org/10.1016/j.csbj.2023.11.056.
31. Yoshida K, Kuroda D, Kiyoshi M, Nakakido M, Nagatoishi S, Soga S, et al. Exploring designability of electrostatic complementarity at an antigen-antibody interface directed by mutagenesis, biophysical analysis, and molecular dynamics simulations. Sci Rep. 2019;9(1):4482. https://doi.org/10.1038/s41598-019-40461-5.
32. Dekkers G, Bentlage AEH, Stegmann TC, Howie HL, Lissenberg-Thunnissen S, Zimring J, et al. Affinity of human IgG subclasses to mouse Fc gamma receptors. MAbs. 2017;9(5):767–73. https://doi.org/10.1080/19420862.2017.1323159.
33. Lux A, Nimmerjahn F. Of mice and men: the need for humanized mouse models to study human IgG activity in vivo. J Clin Immunol. 2013;33(Suppl 1):S4–8. https://doi.org/10.1007/s10875-012-9782-0.
34. Overdijk MB, Verploegen S, Ortiz Buijsse A, Vink T, Leusen JH, Bleeker WK, et al. Crosstalk between human IgG isotypes and murine effector cells. J Immunol. 2012;189(7):3430–8. https://doi.org/10.4049/jimmunol.1200356.
35. Smith P, DiLillo DJ, Bournazos S, Li F, Ravetch JV. Mouse model recapitulating human Fcgamma receptor structural and functional diversity. Proc Natl Acad Sci U S A. 2012;109(16):6181–6. https://doi.org/10.1073/pnas.1203954109.
36. Shultz LD, Ishikawa F, Greiner DL. Humanized mice in translational biomedical research. Nat Rev Immunol. 2007;7(2):118–30. https://doi.org/10.1038/nri2017.
37. Wang-Lin SX, Olson R, Beanan JM, MacDonald U, Balthasar JP, Russo TA. The capsular polysaccharide of acinetobacter baumannii is an obstacle for therapeutic passive immunization strategies. Infect Immun. 2017;85(12). https://doi.org/10.1128/IAI.00591-17.
38. Bamunuarachchi NI, Khan F, Kim YM. Inhibition of virulence factors and biofilm formation of acinetobacter baumannii by Naturally-derived and synthetic drugs. Curr Drug Targets. 2021;22(7):734–59. https://doi.org/10.2174/1389450121666201023122355.
39. Halstead SB, Mahalingam S, Marovich MA, Ubol S, Mosser DM. Intrinsic antibody-dependent enhancement of microbial infection in macrophages: disease regulation by immune complexes. Lancet Infect Dis. 2010;10(10):712–22. https://doi.org/10.1016/S1473-3099(10)70166-3.
40. Qiu H, KuoLee R, Harris G, Van Rooijen N, Patel GB, Chen W. Role of macrophages in early host resistance to respiratory acinetobacter baumannii infection. PLoS ONE. 2012;7(6):e40019. https://doi.org/10.1371/journal.pone.0040019.
41. Chen P, Rayner S, Hu KH. Advances of bioinformatics tools applied in virus epitopes prediction. Virol Sin. 2011;26(1):1–7. https://doi.org/10.1007/s12250-011-3159-4.
42. Abramson J, Adler J, Dunger J, Evans R, Green T, Pritzel A, et al. Accurate structure prediction of biomolecular interactions with alphafold 3. Nature. 2024;630(8016):493–500. https://doi.org/10.1038/s41586-024-07487-w.
43. Masson GR, Jenkins ML, Burke JE. An overview of hydrogen deuterium exchange mass spectrometry (HDX-MS) in drug discovery. Expert Opin Drug Discov. 2017;12(10):981–94. https://doi.org/10.1080/17460441.2017.1363734.
44. Tran MH, Schoeder CT, Schey KL, Meiler J. Computational structure prediction for Antibody-Antigen complexes from Hydrogen-Deuterium exchange mass spectrometry: challenges and outlook. Front Immunol. 2022;13:859964. https://doi.org/10.3389/fimmu.2022.859964.

Publisher's Note